Br-diffusion in molten NaBr explored by coherent quasielastic neutron scattering

F. Demmel,[1,*] O. Alcaraz,[2] and J. Trullas[2]

[1] *ISIS Facility, Rutherford Appleton Laboratory, Didcot, OX11 0QX, UK*
[2] *Departament de Física i Enginyeria Nuclear, Universitat Politècnica de Catalunya, 08034 Barcelona, Spain*

(Dated: January 7, 2016)

Molten sodium bromide has been investigated by quasielastic neutron scattering focusing on the wave vector range around the first structure factor peak. The line width of the scattering function shows a narrowing around the wave number of the structure factor peak, known as deGennes narrowing. In a monatomic system, this narrowing or in the time domain slowing down, has been related to a self-diffusion process of the caged particle. Here we show that this methodology can be applied to the molten alkali halide NaBr. The incoherent scattering from the sodium ions at small wave vectors provides the self-diffusion coefficient of sodium and the dynamics of bromine ions can be studied at wave numbers around the structure factor peak. With input from MD-simulations on the partial structure factors, diffusion coefficients of the bromine ions can be obtained. These experimentally derived diffusion coefficients are in good agreement with molecular dynamics simulation results. This methodology to extract self-diffusion coefficients from coherent quasielastic neutron scattering is applicable to binary fluids in general when one particle dominates the scattering response at the structure factor maximum.

PACS numbers: 61.05.fg, 05.20.Jj, 66.10.-x, 02.70.-c

I. INTRODUCTION

Diffusion is a mass transport process occurring in solids, liquids and gases. Materials science and even life rely on displacements of atoms and molecules due to thermal motion. According to Fick's law the driving force for diffusion is a concentration gradient. This is also the basic principle for the macroscopic measurements of diffusion coefficients, where tracer techniques are applied to determine diffusion coefficients. On a microscopic length scale the motion of a particle is influenced by the collisions with neighboring particles, which can be regarded as a surrounding cage in a dense system. In a fluid this neighboring cage of particles is highly mobile and will influence the probability to diffuse for the caged particle. That correlation between the movement of the tagged particle and surrounding neighbors is evidence that in a dense fluid correlated motions have to be taken into account. For example, in liquid alkali metals it has been demonstrated that the self-diffusion process near the melting point is hindered due to the decay of density fluctuations [1, 2].

On the atomic length scale quasielastic neutron scattering (QENS) is an established method to obtain self-diffusion coefficients. The determination of the motion of a tagged particle needs access to a quantity sensitive to single particle movements. Incoherent neutron scattering provides exactly this tool to extract self-diffusion coefficients from the measured data. However, the prerequisite is that the particle has a large incoherent scattering cross section. That methodology also works in multi-component systems if one particle dominates the incoherent scattering. Yet it would be more fruitful if the coherent scattering could be utilized to provide further information about the diffusion process in the fluid. Here we will demonstrate that in a binary fluid with a particular combination of neutron scattering cross sections the self-diffusion coefficients of both ions can be deduced even though one ion is scattering mainly coherent.

Coherent neutron scattering provides insight into the collective movements of the particles. In the hydrodynamic limit the scattering function of a fluid is given by a combination of three Lorentzians, neglecting a small asymmetry term [3]. Two Brillouin lines originate from density fluctuations and the quasielastic Rayleigh line stems from temperature fluctuations. For larger momentum transfers or when length scales of atomic diameters are probed the quasielastic line shows a narrowing when the structure factor reaches its maximum, known as deGennes narrowing [4]. In the time domain the intermediate scattering function $F(k,t)$ demonstrates a slowing down at the structure factor maximum. DeGennes derived the frequency moments for the scattering function of classical monatomic liquids and found that the second moment is given by: $\omega_0^2 = \frac{k_B T k^2}{mS(k)}$. The moments are a measure of the spread of the spectra and show according to the calculation a decrease of the width around the wave vector k_0 at which the structure factor $S(k)$ reaches its maximum. In a simple picture it costs time for a density fluctuation to relax on a next-neighbor length scale due to a necessary rearrangement of the surrounding particles. This structural slowing down is manifested in the relaxation time through the structure factor $S(k)$.

Within kinetic theory for a dense fluid the linewidth of the scattering function at k_0 has been related to a self-diffusion process, which enables the density fluctuations to decay [5]. Within this formulation the following con-

* franz.demmel@stfc.ac.uk

nection between the Enskog self-diffusion coefficient D_E of a hard sphere fluid and the measured half width at half maximum (HWHM) has been established [5, 6]:

$$\Gamma(k) = \frac{D_E k^2 d(k\sigma)}{S(k)} \tag{1}$$

where $d(k\sigma) = (1 - j_0(k\sigma) + 2j_2(k\sigma))^{-1}$ is given by a combination of spherical Bessel functions j_l of order l and σ denotes the hard sphere diameter. This relation strongly resembles the hydrodynamic description of the self-diffusion process, which is given by $\Gamma(k) = Dk^2$. The structure factor $S(k)$ takes into account the slowing down of a diffusion process at next-neighbor distances and the $d(k\sigma)$ term represents how effective a particle is pushing its neighbors [7]. On these length scales of one atom diameter the relaxation of density fluctuations resembles single particle behavior. It has been shown that the calculated line widths at k_0 of noble gases agree with measured values over a wide range of densities [**?**]. The same relation has also been applied to liquid alkali metals [8, 9], even though the Enskog value is an overestimate compared with simulation results for the self-diffusion coefficient [1, 10]. More recently this methodology was applied successfully to liquid aluminium, a coherent scatterer par excellence for neutrons [11]. All these fluids can be considered in many aspects as models for hard sphere liquids. However, that relation has also been utilized to liquids which are often no more regarded as hard sphere fluids [12, 13].

We will apply this scheme to a binary liquid, molten sodium bromide. There is a long tradition in studying binary ionic liquids and as their prototypes, molten alkali halides, in theory, experiment as well as simulation [14–16], motivated by the obviously simple interatomic potentials in these systems. From the structural point of view, Coulomb liquids exhibit short-range order due to the electrical charges, which are alternating in successive coordination shells around a central [17]. A prominent feature in the dynamics of binary ionic liquids is the prediction of optic-type modes demonstrated in a pioneering molecular dynamics (MD) simulation of a symmetric molten salt by Hansen and McDonald [18]. In the following years the collective particle dynamics of molten salts has been studied, in particular to search for the predicted optic modes, with neutrons [19–22] and with inelastic X-ray scattering [23–26]. That development triggered further simulations on this topic, see for example[27–31].

Transport properties, like diffusion, shear viscosity and ionic conductivity have been studied in parallel through computer simulations [32, 33]. These quantities have a practical significance in e.g. electrochemical devices. On a macroscopic scale diffusion coefficients have been determined through tracer diffusion measurements [34]. A restriction for this method, however, is that convection can influence the results. A method which avoids this complication is quasielastic neutron scattering. However, the extraction of useful information is limited to a small number of ions with appropriate cross sections. One of the examples where the quasielastic neutron scattering was analysed is molten NaI [21]. More recently, the single ion dynamics of molten NaBr was studied thoroughly in a combination of experiment and classical MD-simulation and sodium self-diffusion coefficients were extracted from the experimental data [35]. A good agreement with the MD-simulation results using a point dipole polarised potential was achieved.

Here we will go one step further and demonstrate that also the bromine self-diffusion coefficient can be extracted from the molten sodium bromide data by analysing the deGennes narrowing. In NaBr the coherent signal is dominated by the bromine ion due to the much larger coherent cross section of bromine in comparison to the sodium one. At small momentum transfers the signal is given by the incoherent scattering from sodium and hence the self-diffusion of the sodium ions only can be measured [35]. At larger k-vectors more and more coherent scattering contributions will contribute to the measured signal. Eventually near the first peak of the partial structure factor the scattered intensity stems from the correlations between the particles and due to the size of the cross sections mainly from the bromine ions. At this wave vector according to Eq. 2 the partial structure factor is needed as input, which we use from the MD-simulations. Then we will be able to deduce the bromine self-diffusion coefficient from the experimental data which we will compare to our previous MD-simulation results [35].

II. EXPERIMENTAL AND COMPUTATIONAL DETAILS

The basic variables to describe the dynamic properties of binary charged systems with N_+ cations and N_- anions are the fluctuating local partial number densities of each species with respect to the averaged partial density ρ_a, $\delta\rho_a(\mathbf{r}, t) = \{\Sigma_{ia}\delta[\mathbf{r}\text{-}\mathbf{r}_{ia}(t)]\} - \rho_a$, whose components in the reciprocal space (for wave numbers $\mathbf{k} \neq 0$) are

$$\rho_a(\mathbf{k}, t) = \sum_{ia=1}^{N_a} \rho_{ia}(\mathbf{k}, t) = \sum_{ia=1}^{N_a} \exp[-i\mathbf{k} \cdot \mathbf{r}_{ia}(t)] \tag{2}$$

where a can be either + or −, and $\mathbf{r}_{ia}(t)$ is the position at time t of the ion i_a of species a. Their time correlations are the partial intermediate scattering functions

$$F_{ab}(k, t) = \frac{1}{N} \frac{\langle \rho_a(\mathbf{k}, t)\rho_b(-\mathbf{k}, 0)\rangle}{\sqrt{c_a c_b}} \tag{3}$$

where $N = N_+ + N_-$, $c_a = N_a/N$ and the brackets denote the ensemble average over equilibrium configurations. We define $F_{ab}(k, t)$ as Price and Copley [19] and Rovere and Tosi [15], whose initial time values are the Ashcroft-Langreth partial static structure factors $S_{ab}(k)$. Other authors, e.g. Hansen and McDonald [16] and McGreevy [20], do not include the factor $(c_a c_b)^{-1/2}$. By using this factor, $S_{ab}(k)$ approaches unity as $k \to \infty$.

In a similar vein the self-intermediate scattering function $F^s(k,t)$ is defined as,

$$F_a^s(k,t) = \langle \rho_{ia}(k,t)\rho_{ia}(k,0)\rangle = \frac{1}{N_a}\langle \sum_{ia=1}^{N_a} \exp\{-i\mathbf{k}\cdot[\mathbf{r}_{ia}(t) - \mathbf{r}_{ia}(0)]\}\rangle \quad (4)$$

that is, the autocorrelation of the reciprocal space components of the single particle density $\delta[\mathbf{r}\text{-}\mathbf{r}_{ia}(t)]$. The spectra of $F_{ab}(k,t)$ and $F_a^s(k,t)$ are the partial and self-dynamic structure factors $S_{ab}(k,\omega)$ and $S_a^s(k,\omega)$, respectively.

Inelastic neutron scattering measures the total dynamic structure factor $S(k,\omega)$ of the density fluctuations. Non-magnetic neutron scattering interacts with the nuclei through two cross sections, the incoherent and the coherent one. The incoherent cross section connects with the self-correlations of a single particle and the coherent cross section interferes with correlations between the particles. In general, the double differential cross section per particle is a cross section weighted sum of these two contributions $S_{\mathrm{coh}}(k,\omega)$ and $S^{\mathrm{s}}(k,\omega)$:

$$\frac{d^2\sigma}{d\Omega d\omega} = \frac{k_f}{k_i}[\frac{\sigma_{coh}}{4\pi}S_{coh}(k,\omega) + \frac{\sigma_{inc}}{4\pi}S^s(k,\omega)] = \frac{k_f}{k_i}\frac{\sigma_T}{4\pi}S(k,\omega) \quad (5)$$

where k_i and k_f are the modulus of the incident and scattered neutron wave vectors. In a multi-component system the cross sections are then averaged values: $\sigma_{coh} = 4\pi\sum_a c_a b_a^2$, where b_a is the coherent scattering length of species a, $\sigma_{inc} = \sum_a c_a\sigma_a^{inc}$ and $\sigma_T = \sigma_{coh} + \sigma_{inc}$. In a binary system the measured intensity will consist of five different contributions. The incoherent and coherent dynamic structure factors may be presented as:

$$S_{coh}(k,\omega) = \frac{4\pi}{\sigma_{coh}}\frac{1}{2}[b_{\mathrm{Na}}^2 S_{\mathrm{NaNa}}(k,\omega) + 2b_{\mathrm{Na}}b_{\mathrm{Br}}S_{\mathrm{NaBr}}(k,\omega) + b_{\mathrm{Br}}^2 S_{\mathrm{BrBr}}(k,\omega)] \quad (6)$$

$$S^s(k,\omega) = \frac{1}{\sigma_{inc}}\frac{1}{2}[\frac{\sigma_{\mathrm{Na}}^{inc}}{4\pi}S_{\mathrm{Na}}^s(k,\omega) + \frac{\sigma_{\mathrm{Br}}^{inc}}{4\pi}S_{\mathrm{Br}}^s(k,\omega)] \quad (7)$$

Replacing $S_{ab}(k,\omega)$ and $S_a^s(k,\omega)$ by $F_{ab}(k,t)$ and $F_a^s(k,t)$ in the above equation, we get the coherent and self-intermediate scattering functions $F_{coh}(k,t)$ and $F_s(k,t)$, respectively. The initial value $F_{coh}(k,0)$ is the structure factor $S(k) = \frac{1}{2}[b_+^2 S_{++}(k) + 2b_+b_-S_{+-}(k) + b_-^2 S_{--}(k)]/b^2$ with $b^2 = \sum_a c_a b_a^2 = \sigma_{coh}/4\pi$, in such a way it approaches to unity as $k\to\infty$, and $F^s(k,0) = 1$.

Table I provides the neutron cross sections and the scattering lengths of both ions [36]. Na is a nuclei with nearly equal coherent and incoherent scattering cross section and Br scatters the neutrons mainly coherent.

a	b (fm)	σ_a^{coh} (barn)	σ_a^{inc} (barn)	σ_a^{abs} (barn)
Na	3.6	1.66	1.62	0.53
Br	6.795	5.8	0.1	6.9

TABLE I. Neutron scattering lengths, cross sections and absorption cross sections.

NaBr powder was filled into a flat niobium can and then enclosed through electron beam welding. The niobium wall thickness was 0.5 mm and the sample thickness 3.8 mm, which provided a scattering power of about 12 %. Niobium is a nearly perfect coherent scatterer and hence will not contribute to the elastic line except where Debye-Scherrer lines appear. The first reflection of niobium is at $k = 2.7\ \mathring{A}^{-1}$, which is beyond the first structure factor maximum of molten NaBr ($k \approx 1.7\mathring{A}^{-1}$). The cell was installed under a 45^0 orientation in a transmission geometry into a standard furnace with niobium shields. The measured temperatures were 1043 K, 1123 K and 1223 K for molten NaBr ($T_{melt} = 1000\ K$). The temperature uncertainty was smaller than $\pm 1.5K$ during all measurements. An identical cell was used for empty cell runs.

Quasielastic neutron scattering measurements were performed at the OSIRIS spectrometer of the ISIS facility, UK. This instrument is an indirect time of flight backscattering spectrometer that was operated with a final energy $E_f = 7.38\ meV$ [37]. The energy resolution deduced from a vanadium measurement is 0.099 meV in this configuration. The data analysis included monitor normalisation and empty cell subtraction, taking into account self and can absorption. Absorption coefficients have been calculated according to a method by Paalman and Pings [38]. For a full subtraction of the empty cell contribution a scaling factor of 1.15 had to be included. A conversion to constant k-spectra was performed with a binning in wave vector of $\Delta k = \pm 0.05\mathring{A}^{-1}$. Finally an absolute normalisation was achieved through a comparison with a vanadium measurement. All analysis steps have been performed with the Mantid software framework [39]. To extract the line width a fit with a single Lorentzian function convoluted with the measured resolution function was applied. It has been demonstrated that the lineshape of the coherent scattering function at the structure factor maximum can be approximated by a single Lorentzian [40]. Included into the fit was a linear sloping background, taking care of the faster coherent contributions and if necessary a delta function for not completely subtracted elastic contributions. Fig 1 shows an intensity map of molten NaBr at 1043 K. Towards small k-vectors an increase in the amplitude can be observed, a sign of quasielastic incoherent scattering. This shape demonstrates that the measured signal stems from sodium diffusion within this range of k-vectors. At k-vectors around $k \approx 1.7\mathring{A}^{-1}$ the dynamic structure factor shows a peak due to coherent scattering.

Since σ_{Na}^{inc} is quite large in contrast to σ_{Br}^{inc}, in molten

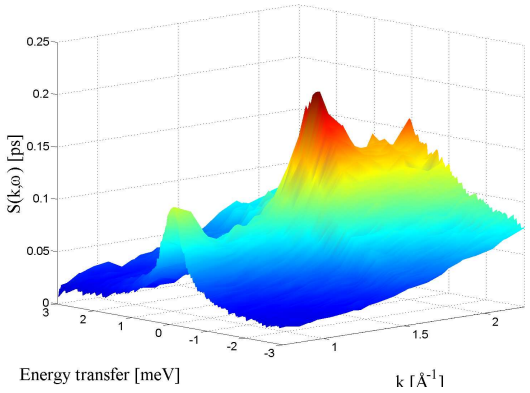

FIG. 1. (Color online) An intensity map against momentum and energy transfer is shown for molten NaBr at 1043 K. Towards small k-vectors a strong increase in amplitude occurs from the incoherent scattering of the sodium ions. The peak at about $k \approx 1.7\mathring{A}^{-1}$ signals the correlations from the bromine ions.

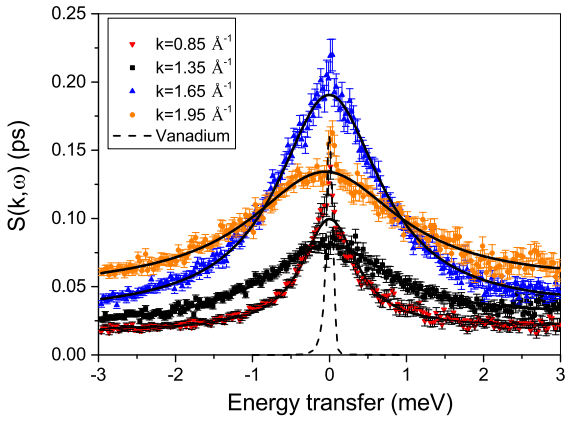

FIG. 2. (Color online) Spectra of molten NaBr are shown for different momentum transfers. Included is the energy resolution from a vanadium scan. The lines depict fits with a Lorentzian function.

NaBr $S^s(k,\omega)$ is practically determined by $S^s_{Na}(k,\omega)$. Furthermore, since $S(k)$ at small wave vectors is much smaller than 1, the coherent contribution at these wave numbers is small and the measured intensity at small momentum transfers is given by the incoherent scattering from sodium and hence the self-diffusion of the sodium ions can be extracted from the relation $\Gamma(k) = D_{Na}k^2$, what has been explored previously. With increasing wave vector, however, the contributions from collective movements will increase the measured signal, which can be seen as the increasing signal with increasing wave vector at non-zero energy transfer. At the peak position $k \approx 1.7\mathring{A}^{-1}$ the main contribution in the dynamic structure factor will come from the coherent scattering of the bromine ions as we will show in the following sections in more detail. Measured spectra of NaBr are displayed in Fig. 2 for a few selected momentum transfers. The lines are fits with a single Lorentzian convoluted with the measured resolution function. Within the measured energy range and k-range a single Lorentzian provides a good fit model to the data.

To complement the data analysis we carried out Molecular Dynamics (MD) simulations using a Polarizable Ion Model (PIM) for molten NaBr constructed by adding the many-body induced polarization interactions to the Fumi-Tosi pair potential [41, 42]. We assume that a point dipole is induced on an ion placed at position r_i as result of two contributions. The first one is the dipole induced by the local electric field E_i due to all other ions, whose moment is given by the electronic polarizability α_i in the linear approximation $\alpha_i E_i$. The second is the short-range damping contribution due to the neighboring ions needed to avoid unphysical over-polarizations. The overall description of a simple PIM is given in [43] and that for PIM with short-range damping interactions in [44]. By using the same potential parameters values as in [35], we simulated molten NaBr at the measured temperatures 1043, 1123 and 1223 K, with densities 0.02716, 0.02645 and 0.02551 ions/$\mathring{A}^3$, respectively [46]. MD-simulations were carried out considering 1000 ions placed in a cubic box of side L with periodic boundary conditions, in such a way that the MD accessible wave vectors are limited to those given by $k = n(2\pi/L)$, where n is a vector of integer components. We use the Beeman's algorithm [42] with a time step of 1 $fs = 10^{-15}$ s over 450000 time steps. This large number of time steps is necessary to reduce the statistical fluctuations in the partial intermediate scattering functions. Other computational details are those in [35].

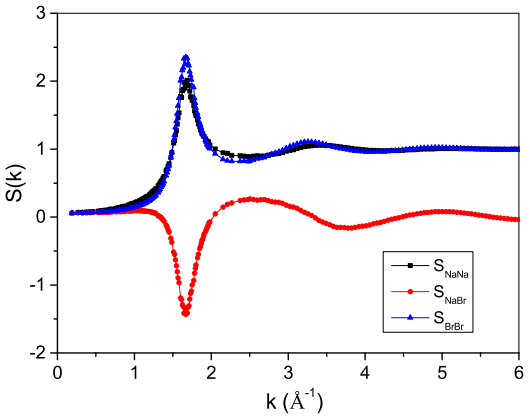

FIG. 3. (Color online) Partial structure factors $S_{ab}(k)$ are presented for the simulation at 1043 K: Na-Na (squares), Na-Br (circles) and Br-Br (triangles).

In figure 3 the partial structure factors $S_{ab}(k)$ are presented for $T = 1043$ K. The peak value of $S_{BrBr}(k)$ is slightly higher than that of $S_{NaNa}(k)$ and hence the

peak width is less broad in wave number. It demonstrates that the bromine ions are slightly more ordered than the smaller sodium ions. The peak value of the partial structure factor of $S_{BrBr}(k)$ occurs at $k_0 = 1.68\ \mathring{A}^{-1}$ and will be used in the subsequent data analysis.

In Fig. 4 we present a comparison of spectra between MD-simulation and QENS for two wave vectors. From the simulation the total dynamic structure factor $S(k,\omega)$ and the incoherent contribution alone $S^s(k,\omega)$ are plotted. There is an overall good agreement between simulation and neutron data on an absolute intensity scale, which underlines the reliability of the simulated data on a quantitative level. No intensity adjustment was made between the experimental and computational spectra. At larger energy transfers the experiment shows a larger intensity compared to the simulation. One reason for this might be that multiple scattering effects have not been corrected in the data or it might be that we see the limitations of the used potential implementation. The influence of multiple scattering effects is wave vector dependent and does not play a significant role at the structure factor maximum, as demonstrated in [9]. Hence, around k_0, where the data are used in our analysis, multiple scattering effects should play only a marginal role for the observed intensity difference. The figure includes also the incoherent part of the total scattered signal. At $k = 0.82\ \mathring{A}^{-1}$ the total signal is dominated by the incoherent contribution, which is here defined by the sodium ions. That confirms our assumption from the previous experiment when we extracted the sodium diffusion coefficient from the small wave vector range [35]. However, at the structure factor peak the intensity stems from the coherent contribution and hence mainly from the bromine correlations.

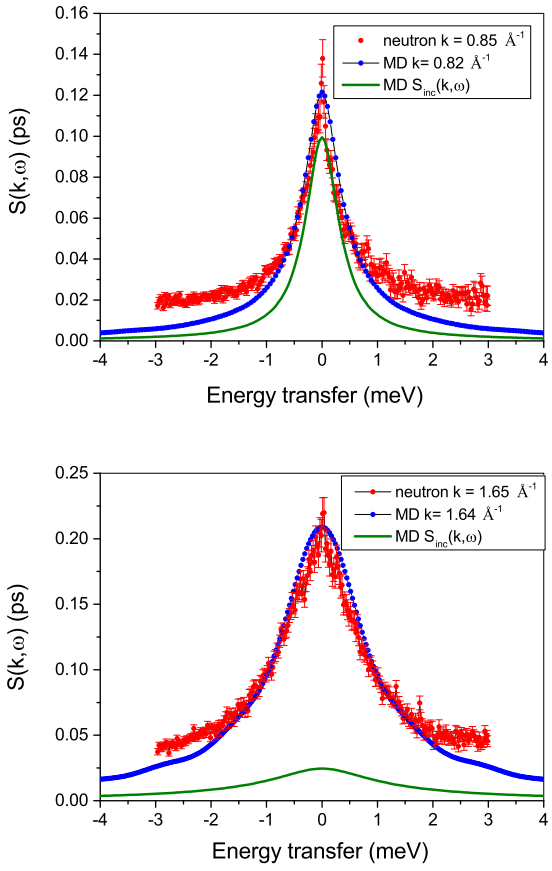

FIG. 4. (Color online) A comparison of neutron spectra and MD-simulation spectra is presented for T=1043 K. At $k = 0.82\ \mathring{A}^{-1}$ the intensity is dominated by the incoherent contribution whereas at $k = 1.65\ \mathring{A}^{-1}$ the signal is mainly of coherent nature.

III. RESULTS AND DISCUSSION

The half width at half maximum $\Gamma(k)$ has been determined through fitting with a Lorentzian model. In Fig. 5 all HWHMs are plotted for the three measured temperatures. The deGennes narrowing is well expressed for all three temperatures. The results from the QENS data around the first structure peak are shown in Fig. 6 in more detail. Included is the energy integrated intensity which is near to the total neutron weighted structure factor $S(k)$, except the part of intensity outside the integration window. When $S(k)$ shows a maximum the width responds with a minimum as expected for the deGennes narrowing.

Within kinetic theory for a monatomic liquid the line width at the structure factor maximum has been related to a self-diffusion process, which enables the density fluctuations to decay (see Eq. 2) [5]. Herein a direct correlation between the Enskog self-diffusion coefficient D_E of a hard sphere fluid and the measured $\Gamma(k)$ has been established. The Enskog approximation is an improvement to the Boltzmann result for diffusion in gases and considers correlations between the particles for systems with larger particle density [3]. At higher densities the collision rate is governed by the product of the particle density with the radial pair correlation function. As already demonstrated the density fluctuation spectrum at k_0 is mostly related to coherent scattering and hence to the bromine movements. Nevertheless at this point there is an approximation when the coherent contribution from the sodium ions, which amounts to about a factor 3 less than the bromine ions according to the scattering length contributions to Eq. 7, is incorporated into the data analysis. From the partial structure factor simulation at 1043 K (see Fig 3) we get $S_{BrBr}(k_0 = 1.68\ \mathring{A}^{-1}) = 2.35$ and from the measurement of the HWHM we obtain $\Gamma = 0.88\ meV$. For the hard sphere diameter of bromine we take the ionic radius from Janz [46] as $2r_{Br} = \sigma_{Br} = 3.9\ \mathring{A}$. With these parameters a bromine diffusion constant $D_E = 8.0 \cdot 10^{-5}\ cm^2/s$ is calculated.

However, the Enskog model calculates the diffusion coefficient D_E of a hard sphere system by taking into ac-

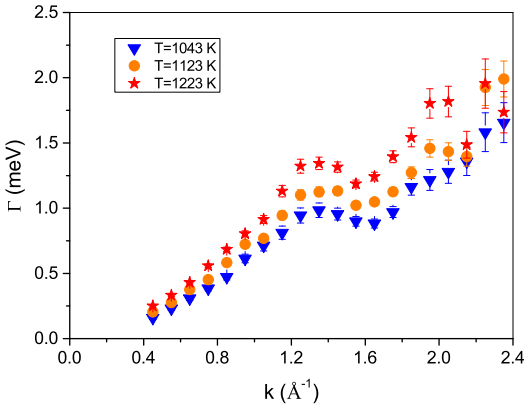

FIG. 5. (Color online) The HWHM's against k are presented for the QENS results for all three temperatures.

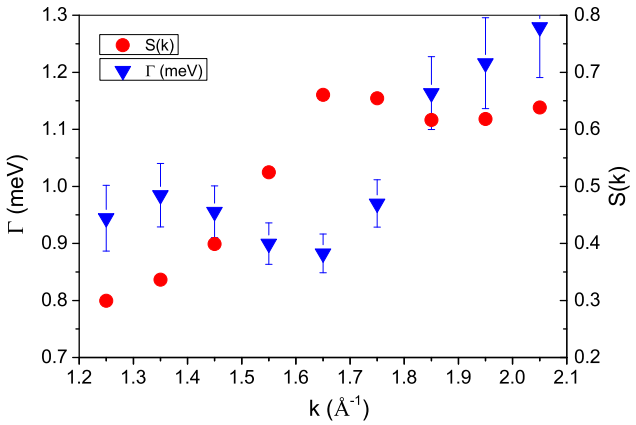

FIG. 6. (Color online) The HWHM against k is presented for the QENS results around the structure factor peak for T=1043 K. Included is the total neutron weighted structure factor $S(k)$ obtained through energy integration of the measured spectra.

count only binary collisions. When the density increases it is no more valid to consider only uncorrelated binary collisions and successive correlated collisions have to be taken into account. The neglect of more complex correlated collisions is the reason for deviations of the macroscopic self-diffusion constant at high and low densities. A kinetic theory with inclusion of correlated collisions has been given first by Cukier and Mehaffey [49] for a hard sphere liquid and later by Wahnstrom and Sjogren [50] for continuous potentials. At high densities coupling to density fluctuations with wave numbers near the structure factor maximum hinder the diffusion process and hence reduce the diffusion constant [10]. In contrast, at low densities it is the coupling to vortex-backflow which enhances the diffusion constants. Through a comparison between simulated self-diffusion coefficients and calculated Enskog-values over a large range of densities a

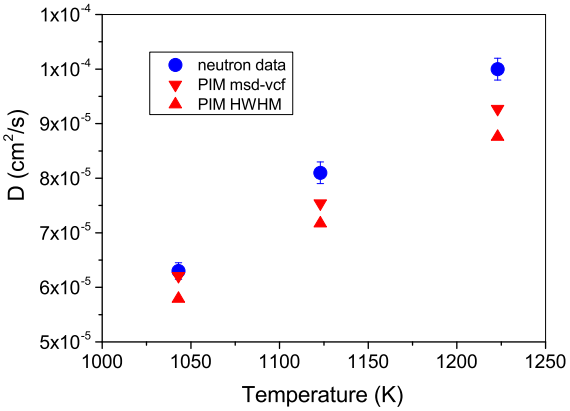

FIG. 7. (Color online) The resulting Br-diffusion coefficients from the coherent QENS data and from the MD-simulation are plotted against the temperature.

correction curve was reported [47]:

$$D = D_E\ (1+0.05403(\frac{V_0}{V})+6.3656(\frac{V_0}{V})^2-10.9425(\frac{V_0}{V})^3) \quad (8)$$

The correction is given as a function of relative density $V_0/V = n\sigma^3/\sqrt{2}$, where V_0 denotes the closed packed volume and n is the particle density. E.g. these corrections describe quantitatively very well the diffusion behavior of liquid sodium over a wide range of densities [48]. The characteristic feature of Eq. 8 is well displayed, namely the reduction of D/D_E near the melting point via the cage-effect and an enhancement of D/D_E due to transverse currents at higher temperatures with a typical maximum near $V_0/V = 0.4$ [2]. We need a hard sphere parameter for a multi particle system which we will calculate according to [51]: $\sigma^3_{ave} = \frac{\sigma^3_{Na}+\sigma^3_{Br}}{2}$. With $\sigma_{Na} = 1.9$ Å and $\sigma_{Br} = 3.9$ Å we obtain a $\sigma_{ave} = 3.2$ Å. With the respective particle density $n = 2\cdot 1.36\cdot 10^{22}\ cm^{-3}$ we calculate the right hand side of Eq. 8 to 0.79. Such a value is quite typical as correction for the Enskog self-diffusion constant near the melting point [2, 47, 48].

With that correction a diffusion coefficient for bromine of $D_{Br} = 6.3\cdot 10^{-5}\ cm^2/s$ is obtained in quite good agreement with the result from the MD-simulation $D_{Br} = 5.8(6.2)\cdot 10^{-5}\ cm^2/s$ [35], where the values are deduced from the HWHMs of the spectra at small wave vectors or from the mean squared displacements (msd), in brackets. Table II provides input parameter and results for all three temperatures. The particle diameter $\sigma_{ave} = 3.2$ Å has been kept constant over this temperature range. In Fig. 7 the resulting Br-diffusion coefficients are plotted together with the results from the MD-simulation [35]. Both results from the evaluation of the mean squared displacements and from an analysis of the HWHM at small k-vectors are displayed. Near the melting point a surprising good agreement can be stated. Such a good

T (K)	$S(k_0)$	n $10^{22}\ cm^{-3}$	D_E $10^{-5}\ cm^2/s$	D $10^{-5}\ cm^2/s$	D_{MD} $10^{-5}\ cm^2/s$
1043	2.35	2.72	8.0	6.3 ± 0.15	5.8(6.2)
1123	2.18	2.64	9.4	8.3 ± 0.2	7.2(7.5)
1223	2.1	2.56	10.8	10.5 ± 0.2	8.8(9.3)

TABLE II. Some input parameters for the data analysis are listed: ion particle density n, peak value for the partial structure factor of bromine $S_{BrBr}(k_0)$, D_E, corrected D and bromine diffusion coefficients from the MD-simulation D_{MD} [35].

agreement might be fortunate and fortuitous for our considered system. On the other hand it might be evidence that binary systems with a good separation in the scattering contributions and a well-defined deGennes narrowing can be used to obtain diffusion coefficients from coherent quasielastic neutron scattering. With rising temperature the Br-diffusion coefficients deviate from the simulation values. This might indicate that the methodology here presented will apply solely to dense hard sphere system and are no more strictly valid with rising temperature and hence reduced particle density. Not excluded is also the possibility that polarization effects in the interaction potential show a subtle change with reduced density.

IV. CONCLUSIONS

We conducted a quasielastic neutron scattering experiment on molten NaBr focusing on the wave vector range around the first structure factor peak. At small wave vectors the translational self-diffusion of the sodium ions can be measured [35], because the incoherent scattering is dominated by the sodium ions. In contrast, bromine is the dominating coherent neutron scattering ion in this compound and the scattered intensity at the first structure factor peak stems mainly from bromine movements. The HWHMs at these wave vectors, known as deGennes narrowing, can be related to a self-diffusion process. The accompanying MD-simulations, using a classical Fumi-Tosi potential extended to include the bromine polarization, shows a good agreement with the experimental data on a quantitative level with respect to spectral lineshape and linewidth. With the input of the partial structure factor from the MD-simulation a self-diffusion coefficient can be deduced from the mainly coherent scattering process. These diffusion coefficients have been corrected for processes beyond binary collisions events. The resulting final diffusion coefficients are in remarkable good agreement with the results from the MD-simulation, computed at small wave vectors. The presented analysis demonstrates that also in binary or even multi-component fluids more than one self-diffusion coefficient can be extracted experimentally. The prerequisites are a distinct difference in neutron cross sections, a well expressed deGennes narrowing and the particle can still be regarded as hard-sphere-like. Furthermore the relaxation of the density fluctuations at the structure factor maximum should be governed by one particle component, enabled through a large difference in size for example, which renders this process to a one component relaxation. If then partial structure factors are available the presented methodology can be applied.

ACKNOWLEDGEMENTS

O. Alcaraz and J. Trullàs thank the grants No. FIS20012-39443-C02-01 from MINECO of Spain and No. 2012SGR-39443 from Generalitat de Catalunya. We are grateful to the ISIS furnace section for the excellent support and to the ISIS Facility for the provision of beam time. This work was partly supported by the Science and Technology Facilities Council, STFC.

[1] U. Balucani, A. Torcini and R Vallauri, Phys. Rev. B **47** 3011 (1993)
[2] C. Morkel and W.-C. Pilgrim, J of Non-Cryst **312-314**
[3] J.P. Boon and S. Yip, *Molecular Hydrodynamics*, McGraw Hill (1980)
[4] P.G. deGennes, Physica **25** 825 (1959)
[5] E.G.D. Cohen, P. Westerhuijs and I. M. de Schepper, Phys. Rev. Lett. **59** 2872 (1987); E.G.D. Cohen, I. M. de Schepper and M.J. Zuilhof, Physica B **127** 282 (1984)
[6] T.R. Kirkpatrick, Phys. Rev. A **32** 3130 (1985)
[7] W. Montfrooij and I. deSchepper *Excitations in simple liquids, liquid metals and superfluids* (Oxford University Press, Oxford, 2010)
[8] T. Bodensteiner, C. Morkel, W. Gläser and B. Dorner, Phys. Rev. A **45**, 5709 (1992)
[9] F. Demmel, A. Diepold, H. Aschauer and C. Morkel, Phys. Rev. B **73**, 104207 (2006)
[10] U. Balucani and M. Zoppi, *Dynamics of the Liquid State*, Clarendon Press, Oxford (1994)
[11] F. Demmel, D. Szubrin, W-C Pilgrim and C. Morkel, Phys. Rev. B **84**, 014307 (2011)
[12] Y. Baydal, U. Bafile, K. Miyazaki, I. M. deSchepper and W. Montfrooij, Phys. Rev. E **68**, 061208 (2003)
[13] T. Scopigno, R. Di Leonardo, L. Comez, A.Q.R. Baron, D.Fioretto and G. Ruocco, Phys. Rev. Lett. **94**, 0155301 (2005)
[14] N.H. March and M.P. Tosi *Coulomb Liquids* Academic Press, San Diego (1984)
[15] M. Rovere and M.P. Tosi, Rep. Prog. Phys. **49**, 1001 (1986)

[16] J.P. Hansen and I. McDonald *Theory of simple liquids* Academic Press, London (2006)

[17] F.G. Edwards, J.E. Enderby, R.A. Howe and D. I. Page, J.Phys. C**8** 3483 (1975); J. Locke, S. Messoloras, R. J. Stewart, R. L. McGreevy and E. W. J. Mitchell, Phil. Mag. B **51** 301 (1985); M. A. Howe, R. L. McGreevy and W. S. Howells, J. Phys.: Condens. Matter **1** 3433 (1989)

[18] J.P. Hansen and I.R. McDonald, Phys. Rev. A **11** 2111 (1975)

[19] D.L. Price and J.R.D. Copley, Phys. Rev. A **11** 2124 (1975)

[20] R.L. McGreevy, Solid State Physics **40** 247 (1987)

[21] R.L. McGreevy, E.W.J. Mitchell and F.M.A. Margaca, J Phys C **17** 775 (1984)

[22] F. Demmel, D. Szubrin, W.C. Pilgrim, A. De Francesco and F. Formisano, Phys Rev E **92** 012307 (2015)

[23] F. Demmel, S. Hosokawa, M. Lorenzen and W.-C. Pilgrim, Phys Rev B **69** 012203 (2004)

[24] M. Inui, S. Hosokawa, Y. Kajihara, K. Matsuda, S. Tsutsui and A.Q.R. Baron, J. Phys.: Condens. Matter **19** 466110 (2007)

[25] F. Demmel, S. Hosokawa and W.-C. Pilgrim, J Alloys Comp **452** 143 (2008)

[26] S. Hosokawa, F. Demmel, W.-C. Pilgrim, M. Inui, S. Tsutsui and A. Baron, Electrochemistry **77** 608 (2009)

[27] T. Bryk and I. Mryglod, Phys. Rev. B **71** 132202 (2005)

[28] T. Bryk and I. Mryglod, Phys. Rev. B **79** 184206 (2009)

[29] O. Alcaraz and J. Trullas, J. Mol. Liqu. **136** 227 (2007)

[30] O. Alcaraz, V. Bitrian and J. Trullas, J. Chem. Phys. **127** 154508 (2007)

[31] O. Alcaraz and J. Trullas, J. Chem Phys **132** 054503 (2010)

[32] G. Ciccotti, G. Jacucci and I.R. McDonald Phys. Rev. A **13**, 426 (1976).

[33] G. Jacucci, I.R. McDonald and A Rahman Phys. Rev. A **13**, 1581 (1976).

[34] J.O. Bockris and G.W. Hooper, Discuss Faraday Soc **32** 218 (1961)

[35] O. Alcaraz, F. Demmel and J. Trullas, J. Chem Phys **141** 244508 (2014)

[36] V.F. Sears, Neutron News, Vol. **3**, No. 3, (1992) pp. 29-37

[37] M.T.F. Telling and K.H. Andersen, Phys Chem Chem Phys **7** 1255 (2005); F. Demmel and K. Pokhilchuk, Nucl Instr and Meth A **767** 426 (2014)

[38] H.H. Paalman and C.J. Pings, J. of Appl. Phys. **33** 2635 (1962)

[39] http://www.mantidproject.org

[40] U. Balucani and R. Vallauri Phys. Rev. A **40** 2796 (1989)

[41] M.P. Tosi and F.G. Fumi, J Phys Chem Solids **25** 45 (1964)

[42] M.J.L. Sangster and M. Dixon, Adv. Phys. **25** 247 (1976)

[43] J. Trullas, O. Alcaraz, L.E. Gonzalez and M. Silbert, J. Phys. Chem. B **107**, 282 (2003)

[44] V. Bitrian and J. Trullas, J. Phys. Chem. B **110** 7490 (2006)

[45] F. J. Vesely, J. Comput. Phys. **24**, 361 (1977)

[46] G.J. Janz, *Molten Salts Handbook*, Academic Press, New York (1967)

[47] J.J. Erpenbeck and W.W. Wood, Phys Rev A **43** 4254 (1991)

[48] W.-C. Pilgrim and C. Morkel, J. Phys.: Condens Matter **18** R585 (2006)

[49] R.I. Cukier and J.R. Mehaffey, Phys Rev A **18** 1202 (1978)

[50] G. Wahnstrom and L. Sjogren, J.Phys.C: Solid State Phys. **15** 401 (1982)

[51] J.A. Barker and D. Henderson, Rev. Mod. Phys. **48** 587 (1976)